IARJSET ISSN (O) 2393-8021, ISSN (P) 2394-1588

International Advanced Research Journal in Science, Engineering and Technology

Impact Factor 8.066 ⁜ Peer-reviewed / Refereed journal ⁜ Vol. 11, Issue 12, December 2024

DOI: 10.17148/IARJSET.2024.111201

# NUMERICAL INVESTIGATION OF TURBULENT FLUID FLOW OVER A POROUS AEROFOIL WING DESIGN WITHIN A MAGNETIC FIELD

**Kirui G. K[1], Mukuna W. O[2], Oduor M. O[3]**

Department of Mathematics, Actuarial and Physical Science, University of Kabianga, P.O.Box 2030-20200

Kericho, Kenya[1,2,3]

**Abstract:** A mathematical model of turbulent fluid flow over a porous aerofoil wing design within a magnetic field is considered. The fluid flow was modelled using Navier stokes equations of conservation of momentum, energy and mass in cylindrical coordinates. The governing equations were then non-dimentionalized and gave rise to the non-dimensional parameters. Computational fluid dynamics (CFD) techniques was used to simulate the flow of air over a porous wing within a range of magnetic field strengths. Examinations of the effects of the magnetic field on key performance metrics such as lift, drag, and efficiency, as well as the overall flow structure of the wing was performed and found valuable insights into the use of porous aerofoil wings in the design of aircraft operating in high-magnetic field environments, such as those found in space or near the Earth's poles. Additionally, the outcomes of the research had wider implications for other domains investigating the impact of magnetic fields on fluid motion, such as in the design of magnetic resonance imaging systems or in the study of planetary motions. Aerofoil wings are an essential component of aircraft design, as they provide lift and enable flight. However, the flow of air over the wing is often turbulent, which can lead to decreased efficiency and performance. Porous aerofoil wings was proposed as a means of reducing turbulence, and the effects of such wings on fluid flow within a magnetic field have been thoroughly investigated. In this research, numerical investigation of the effects of a magnetic field on turbulent fluid flow over a porous aerofoil wing design was done. It is evident from the results that the primary velocities increase when the magnetic parameter was reduced. It was also found that the lift force increases when the Grashof number and Prandtl number decreases.

**Keywords:** Turbulent, Porous medium, Aerofoil, Prandtl number, Magneto hydrodynamics.

## I. INTRODUCTION

The study of turbulent fluid flow over aerofoil wings is an important area of research in the field of aerospace engineering, as it has the potential to improve the performance and efficiency of aircraft Klose, *at el* (2018). Turbulent is a type of fluid flow characterized by chaotic, turbulent eddies and fluctuations in velocity and pressure, and it can lead to decreased lift and increased drag, reducing the overall performance of the wing. In this study, we conducted a numerical exploration of the influence of a magnetic field on turbulent fluid flow through a porous wing design. Pore size of less than 5mm in diameter was uniformly spaced at 5mm on the wings. We used computational fluid dynamics (CFD) techniques to simulate the flow of air over a porous wing within a range of magnetic field strengths, examined the effects on key performance metrics such as lift, drag, and efficiency, as well as the overall flow structure of the wing. The use of CFD in this study enabled us to effectively model and analyze the fluid flow over the wing in a computationally efficient manner. We used a range of CFD models, including Reynolds-averaged Navier-Stokes (RANS) and large-eddy simulation (LES), to capture the effects of turbulence on the flow. We also considered the use of different porous media models to accurately represent the flow through the porous region of the wing. This study has provided valuable insights into the use of porous aerofoil wings in the design of aircraft operating in high-magnetic field environments. Furthermore, the results of this study could potentially be applied to other fields where the effects of a magnetic field on fluid flow are of interest, such as in the design of magnetic resonance imaging systems or in the study of planetary atmospheres. Magneto Hydrodynamics, explores the interaction of fluids and magnetic fields at low frequencies, assuming minimal Maxwell bias and treating fluid as a continuum Cortés-Dominguez, (2018). Kim et al., (2021) A CFD study on flow control of ammonia injection for denitrification processes of SCR systems in coal-fired power plants. This literature review provides an overview of the experimental and numerical studies that have been conducted on the flow over porous surfaces, including the different types of porous media models that have been used and the experimental techniques that have been employed. Chen *et al*., (2016) used numerical analysis to examine the impact of a porous surface on the performance of a transonic airfoil and to gain insights into the mechanism of passive shock/boundary layer interactions.

 

IARJSET ISSN (O) 2393-8021, ISSN (P) 2394-1588

International Advanced Research Journal in Science, Engineering and Technology

Impact Factor 8.066 ⁜ Peer-reviewed / Refereed journal ⁜ Vol. 11, Issue 12, December 2024

DOI: 10.17148/IARJSET.2024.111201

### 1.1 Fundamental Fluid Dynamic Concepts

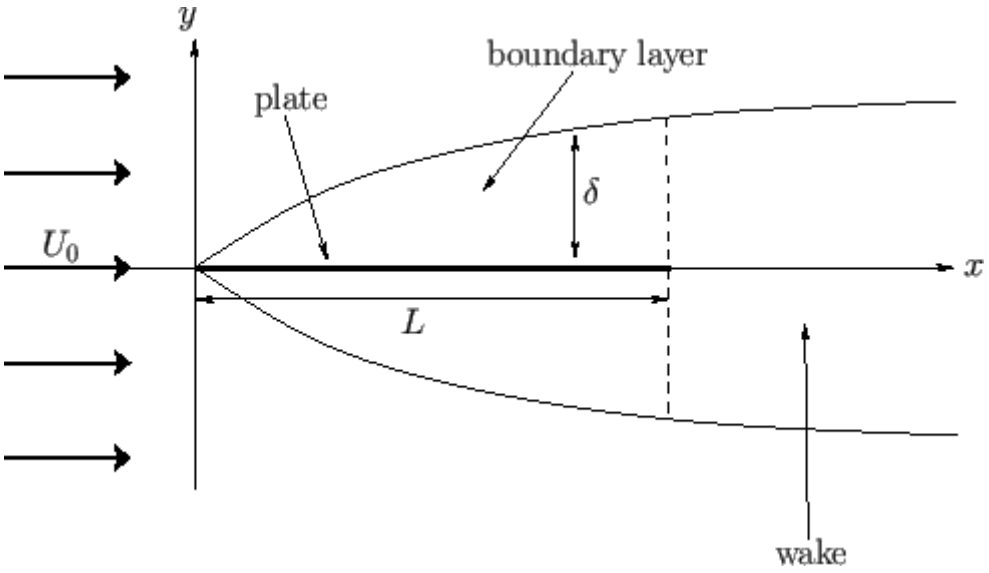


Figure 1.2 Flow over a flat plate

### 1.2 Turbulent Fluid Flow

The Reynolds number is one of the metrics employed to distinguish laminar from turbulent fluid flow. A flow is considered laminar if the Reynolds number is up to 2300, and the properties of the fluid at each point of the flow remain constant--including velocity and pressure since viscous force is more prominent due to the slower flow rate. A flow is considered turbulent if the Reynolds number is greater than 3500. A faster and irregular flow path maximizes the inertial force in the system. Unlike laminar flow, the fluid layers in turbulent flow can cross paths due to the continuous change in the magnitude and direction of the flow. Eddies or swirls can be observed in turbulent flow, and the apparent erratic flow behavior makes the analysis of turbulent flow a challenge. However, despite the challenges, turbulent flow analysis is important for industries, as most flows observed are turbulent. Due to the turbulence of the liquid, the momentum of the liquid changes over time, which is equal to the force generated at a certain distance. The change in velocity, that is, the properties of the fluid for a given point per unit of time in the system, causes periodic turbulence. Reynolds number(Re) increases proportionally with increasing fluid turbulence. In aviation, aerofoils are used to alter airflow in order to create lift. The aerofoil has a curved leading edge and a pointed trailing edge. Additionally, it has an upper and bottom surface. Straight line drawn from the trailing edge to the leading edge is the chord line. Angle of Attack is the angle between the chord line and the flow of relative wind. The angle of attack may be modified based on the situation. The flow across the aerofoil wings of NACA 6412, 7412, and 8412 has been examined by (Manda *et al.*,2020). The analysis concluded that the aerofoil wing of 8412 has shown a better flow separation. Alsahlan, (2017) conducted a study on Aerofoil Design for Unmanned High-Altitude Aft-Swept Flying Wings. Keshri, (2018) looked into unsteady magneto-convection in the presence of buoyant pressures. Also Amrit*et al*, (2018) presented methodology for exploring trade-offs in aerodynamic design using a trust-region-based, multi-fidelity optimization algorithm

### 1.3 Magnetic Field Effect on Fluid Flow

The problem of free convective Magnetohydrodynamic fluids is of great interest in such industries as MHD accelerators, aeromagnetic hydrodynamics, and space technologies such as celestial bodies. The field of petroleum technologies for cleaning and filtration processes in chemical engineering using the effect of oil flow through porous rocks, convection flow without MHD through a porous medium, Chebos *et al*., (2016). The magnetic field is created automatically by the moving charge, and the fluctuating magnetic field induces the Hall current. When researching the influence of magnetic fields on the temperature distribution of electrically conducting liquids, the Hall Effect is of significant interest. Magnetohydrodynamic(MHD) is the study of the flow of electrically conducting fluids in the presence of a magnetic fieldBlakey-Milner, *et al* (2021). Joshi, *et al*, (2016) provides an overview of the existing knowledge and understanding of the interactions between porous aerofoil wings, magnetic fields, and turbulent fluid flow. "Flow over porous bird wings and non-flapping" Aldheeb et al., (2016), including the different types of porous media models that have been developed, the effects of various parameters on the flow, and the experimental techniques that have been used to study the flow.

IARJSET ISSN (O) 2393-8021, ISSN (P) 2394-1588

International Advanced Research Journal in Science, Engineering and Technology

Impact Factor 8.066 ⁜ Peer-reviewed / Refereed journal ⁜ Vol. 11, Issue 12, December 2024

DOI: 10.17148/IARJSET.2024.111201

### 1.4 Numerical Solution of Turbulent Fluid Flow

Turbulent modeling and simulation is the key to solving fluid flow numerically because most practical fluid flows are turbulent. CFD is the art of rewriting the governing partial differential equations of fluid flow with numbers and advancing these numbers through space and time to produce a comprehensive numerical description of the flow field. Computational issues require the manipulation and solution of numbers. It can be stated that the output of CFD is a collection of numbers accompanied by extensive analysis and discussion. When the turbulent model is combined with the control equation, terms like turbulent viscosity and turbulent thermal diffusivity are transformed into their laminar equivalents. The dimensionless and non-linear control equations for the partial differential will be sampled along with additional terms by the finite difference method and solved into a numerical solution with the help of mathematical computer software. Flow visualization uncovered that the use of porous media on the suction side of the airfoil decreased the flow velocity circulation, disrupted vortex formation, and weakened the vortex energy of various modes Ahmed, (2013).

## II. MATHEMATICAL MODEL

Turbulent unsteady MHD flow over a porous aerofoil wing within a magnetic field is consider. The flow is considered in a 2 –Dimensional cylindrical geometry. The porous wing is assumed to have non-end effects. The porous wing is taken to be along the x- axis and the streamline body to be along the y-axis while the z-axis is taken normal to the porous aerofoil wing. The fluid to be use is air. The fluid flow is along a horizontal infinitely long porous aerofoil wing lying in the x-y plane. The porous aerofoil wing is immersed in the ionized air. The axis of the porous wing is in the positive z-axis direction and the air flows through it in positive z-axis direction parallel to the axis of the wing. OpenFOAM was used to simulate the flow of air over a porous aerofoil wing within a range of magnetic field strengths. The wing was modeled as a two-dimensional section, with the flow of air occurring in the plane of the wing. The porous region of the wing was modeled using a porous media model, with the properties of the porous region (such as porosity and permeability) varied to represent different porous wing designs. This ionized air is assumed to be incompressible and viscous in the magnetic field. A strong magnetic field of uniform strength is applied normal to the direction of flow of the ionized air. The induced magnetic field is considered negligible and the plane is flying horizontal in air hence the force acting on the wings due to gravity is assumed to be zero as in figure 4.2. Simulation of the flow of air over the wing at a range of angles of attack was done, to examine the effects of the magnetic field on lift and drag. Also examination of the overall flow structure over the wing, including velocity and pressure profiles and the presence of turbulent eddies was done.

### 2.1 Geometry of the Problem

3-D geometry of porous wing of NACA aero plane were drawn with scaled in ANSYS Design Modular with aerofoil NACA 2415. The chord length of aerofoil used 100mm for profile (root) and 18mm for wing-tip. Total span length was 177mm with dihedral angle $60^0$.

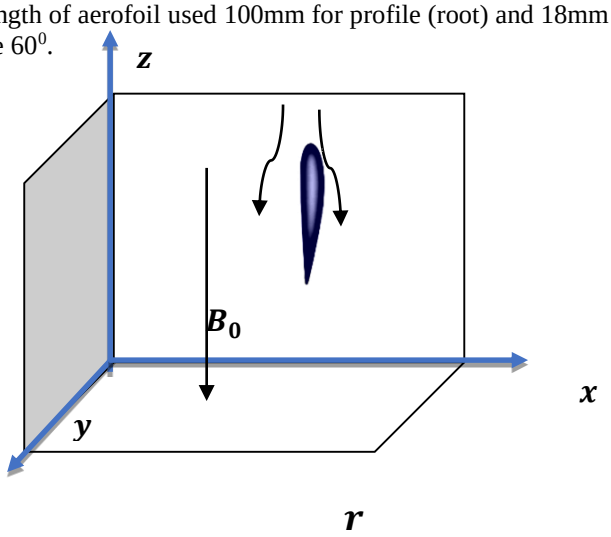


Figure 4.1 PorousWings with NACA 2415

Given that the flow is over porous wing, cylindrical coordinate form of the governing equations discussed in chapter 3 are used. The flow is considered to be along the axial and angular components. There is no radial flow. Thus the two dimensions of this flow are z and θ. From the geometry of the problem above, the porous airfoil wing is infinite such that the derivatives along r and θ are identically zero, more so there is no gravity force acting on the porous wing

IARJSET ISSN (O) 2393-8021, ISSN (P) 2394-1588

International Advanced Research Journal in Science, Engineering and Technology

Impact Factor 8.066 ⁜ Peer-reviewed / Refereed journal ⁜ Vol. 11, Issue 12, December 2024

DOI: 10.17148/IARJSET.2024.111201

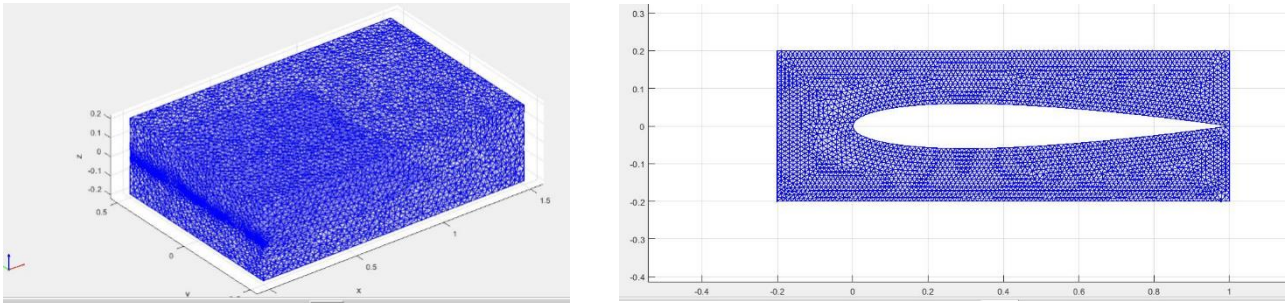

(a) Side view (b) front view

Figure 4.2 Grid generations of Porous Wings

The above flow is governed by the following cylindrical coordinate equations:

$$\frac{\partial \overline{U_z}}{\partial t} = -\frac{1}{\rho}\frac{\partial \overline{P}}{\partial z} + \nu\left(\frac{\partial^2 U_z}{\partial r^2} + \frac{1}{r}\frac{\partial U_z}{\partial r}\right) - \left[\frac{1}{r}\frac{\partial \overline{U_z' U_r'}}{\partial r}\right] + \rho g + \vec{J} \times |_z \quad (1)$$

$$\frac{\partial \overline{U_\theta^*}}{\partial t^*} = V\left(\frac{\partial^2 \overline{U_\theta^*}}{\partial r^{*2}} + \frac{1}{r^*}\frac{\partial \overline{U_\theta^*}}{\partial r^*} - \frac{\overline{U_\theta^*}}{r^{*2}}\right) - \left[\frac{\partial \overline{U_r' U_\theta'}}{\partial r^*} - \frac{2\overline{U_\theta' U_r'}}{r^*}\right] + \vec{J} \times B|_\theta \quad (2)$$

$$\rho C_p\left(\frac{\partial \overline{T^*}}{\partial t^*}\right) = k\left(\frac{\partial^2 \overline{T^*}}{\partial r^{*2}} + \frac{1}{r^*}\frac{\partial \overline{T^*}}{\partial r^*}\right) - \rho C_p\left(\frac{\partial\left(\overline{U_r' T'}\right)}{\partial r^*}\right) \quad (3)$$

It was noted that there was no pressure gradient in $\theta -$ direction and there is no gravitational force also. The boundary and initial conditions are:

$t^* < 0: U_z^* = 0, U_\theta^* = 0, T^* = T_\infty^*$, everywhere (4)

$t^* \geq 0: U_z^* = U_0, U_\theta^* = 0, T^* = T_W^*$, at $r^* = \frac{L}{2}$ ( is the chord Length of the porous aerofoil wing) (5)

$U_z^* \to 0, U_\theta^* \to 0, T^* \to T_\infty^*$, as $r^* \to \infty$ (6)

The pressure gradient in the $z$-axis direction results from the change in elevation up the porous wing. Thus:

$$\frac{\partial P}{\partial z} = -p_\infty g$$

Hence equation (1) becomes:

$$\rho\frac{\partial \overline{U_z}}{\partial t} = (\rho_\infty - \rho)g + \mu\left(\frac{\partial^2 U_z}{\partial r^2} + \frac{1}{r}\frac{\partial U_z}{\partial r}\right) - \rho\left[\frac{1}{r}\frac{\partial \overline{U_z' U_r'}}{\partial r}\right] + \vec{J} \times B|_z \quad (7)$$

The density difference $\rho - \rho_\infty$ may be expressed in terms ofthe volume coefcient of expansion $\beta$ defined by:

$\beta = \frac{1}{V}\left(\frac{\partial V}{\partial T}\right)_P = \frac{1}{V_\infty} \cdot \frac{V - V_\infty}{T - T_\infty} = \frac{p_\infty - p}{p(T - T_\infty)}$ (Frost,2013)

Which simplifies to

$$\frac{\partial \overline{U_z}}{\partial t} = \beta g(T - T_\infty) + \nu\left(\frac{\partial^2 U_z}{\partial r^2} + \frac{1}{r}\frac{\partial U_z}{\partial r}\right) - \left[\frac{1}{r}\frac{\partial \overline{U_z' U'}}{\partial r}\right] + \vec{J} \times B|_z \quad (8)$$

Using $(^*)$ to indicate dimension, equation (4.9) becomes.

IARJSET ISSN (O) 2393-8021, ISSN (P) 2394-1588

International Advanced Research Journal in Science, Engineering and Technology

Impact Factor 8.066 ⁜ Peer-reviewed / Refereed journal ⁜ Vol. 11, Issue 12, December 2024

DOI: 10.17148/IARJSET.2024.111201

$$\frac{\partial U_Z^*}{\partial t^*} = \beta g(T^* - T_\infty^*) + V\left(\frac{\partial^2 \overline{U_{zz}^*}}{\partial r^{*2}} + \frac{1}{r^*}\frac{\partial \overline{U_z^*}}{\partial r^*}\right) - \left[\frac{1}{r^*}\frac{\partial \overline{U_z' U_r'}}{\partial r^*}\right] + \vec{J} \times B|_z \quad (9)$$

We seek to establish the components of the electromagnetic force term in (4.10) and (4.2) that is the term: $\vec{J} \times \vec{B}$

The equation of conservation of charge $\nabla . J = 0$, gives $j_r = k$, a constant, where $\vec{J} = (j_r, j_\theta, j_Z)$ . The constant is zero since, $j_r = 0$ at the aerofoil wing which is porous. Thus $j_r = 0$ everywhere in the flow. Neglecting the ion-slip and thermoelectric eff ects, generalized Ohm's law including the effects of Hall current gives:

$$\vec{J} + \frac{w_e \tau_e}{H_0}(\vec{J} \times \vec{H}) = \sigma(\vec{E} + \mu_0 \vec{q} \times \vec{H} + \frac{1}{e n_e} \nabla P_e) \quad (10)$$

Given that $\vec{H} = (H_0, 0, 0)$ and taking $\vec{J} = (0, j_\theta, j_z), \vec{q} = (0, U_\theta, U_z)$ and $\vec{B} = \mu_0 \vec{H}$simplifying equation (4.12) and solving gives:

$$j_r = 0 \quad (11)$$

$$j_\theta = \frac{\sigma \mu_0 H_0 (U_Z + m U_\theta)}{1 + m^2} \quad (12)$$

$$j_Z = \frac{\sigma \mu_0 H_0 (m U_Z - U_\theta)}{1 + m^2} \quad (13)$$

Where $m = w_e \tau_e$ is the Hall parameter.

Thus the electromagnetic force along $\theta$ and $z$-axis are respectively:

$$(I \times B)_\theta = \frac{\sigma \mu_0^2 H_0^2 (m U_Z - U_\theta)}{1 + m^2} \quad (14)$$

$$(J \times B)_z = \frac{-\sigma \mu_0^2 H_0^2 (U_Z + m U_\theta)}{1 + m^2} \quad (15)$$

Hence the governing equations (1) and (2) are respectively:

$$\frac{\partial \overline{U_z^*}}{\partial t^*} = V\left(\frac{\partial^2 \overline{U_{zz}^*}}{\partial r^{*2}} + \frac{1}{r^*}\frac{\partial \overline{U_z^*}}{\partial r^*}\right) - \left[\frac{1}{r^*}\frac{\partial \overline{U_z' U_r'}}{\partial r^*}\right] + \beta g(T^* - T_\infty^*) - \frac{\sigma \mu_0^2 H_0^2 (\overline{U_z^*} + m \overline{U_\theta^*})}{1 + m^2} \quad (16)$$

$$\frac{\partial \overline{U_\theta^*}}{\partial t^*} = V\left(\frac{\partial^2 \overline{U_\theta^*}}{\partial r^{*2}} + \frac{1}{r^*}\frac{\partial \overline{U_\theta^*}}{\partial r^*} - \frac{\overline{U_\theta^*}}{r^{*2}}\right) - \left[\frac{\partial \overline{U_r' U_\theta'}}{\partial r^*} - \frac{2\overline{U_\theta' U_r'}}{r^*}\right] + \frac{\sigma \mu_0^2 H_0^2 (m \overline{U_z^*} - \overline{U_\theta^*})}{1 + m^2} \quad (17)$$

**2.2 Non-Dimensionalization**

We seek to non-dimensionalize equations (3), (16) and (17). The following scaling variables are applied in the non-dimensionalization process:

$$t = \frac{t^* U_0^2}{v} \qquad r = \frac{r^* U_0}{v} \; U_i = \frac{U_i^*}{U_0}; \theta = \frac{T^* - T_\infty^*}{T_w^* - T_\infty^*} \quad (18)$$

The $(^*)$ superscript denotes the dimensional variables, $U_o$ is the reference velocity, $L$ is the chord length of the porous aerofoil wing, $T_w^* - T_\infty^*$ is the temperature difference between the surface and the free stream temperature.

Using the scaling variables above yields the following equations:

$$\frac{\partial U^*}{\partial t^*} = \frac{\partial U^*}{\partial U}\frac{\partial U}{\partial t}\frac{\partial t}{\partial t^*} = \frac{U_0^3}{v}\frac{\partial U}{\partial t} \quad (19)$$

$$\frac{\partial V^*}{\partial t^*} = \frac{\partial V^*}{\partial V}\frac{\partial V}{\partial t}\frac{\partial t}{\partial t^*} = \frac{V_0^3}{v}\frac{\partial V}{\partial t} \quad (20)$$

IARJSET ISSN (O) 2393-8021, ISSN (P) 2394-1588

International Advanced Research Journal in Science, Engineering and Technology

Impact Factor 8.066 ⁜ Peer-reviewed / Refereed journal ⁜ Vol. 11, Issue 12, December 2024

DOI: 10.17148/IARJSET.2024.111201

$$\frac{\partial U^*}{\partial z^*} = \frac{\partial U^*}{\partial U}\frac{\partial U}{\partial z}\frac{\partial z}{\partial z^*} = \frac{U_0^2}{v}\frac{\partial U}{\partial z} \quad (21)$$

$$\frac{\partial V^*}{\partial z^*} = \frac{\partial V^*}{\partial V}\frac{\partial V}{\partial z}\frac{\partial z}{\partial z^*} = \frac{U_0^2}{v}\frac{\partial V}{\partial z} \quad (22)$$

$$\frac{\partial T^*}{\partial t^*} = \frac{\partial T^*}{\partial \theta}\frac{\partial \theta}{\partial t}\frac{\partial t}{\partial t^*} = (T_w^* - T_\infty^*)\frac{U_0^2}{v}\frac{\partial \theta}{\partial t} \quad (23)$$

$$\frac{\partial^2 U^*}{\partial z^{*2}} = \frac{\partial}{\partial z}\left(\frac{U_0^2}{v}\frac{\partial U}{\partial z}\right)\frac{\partial z}{\partial z^*} = \frac{U_0^3}{v^2}\frac{\partial^2 U}{\partial z^2} \quad (24)$$

$$\frac{\partial^2 V^*}{\partial z^{*2}} = \frac{\partial}{\partial z}\left(\frac{U_0^2}{v}\frac{\partial V}{\partial z}\right)\frac{\partial z}{\partial z^*} = \frac{U_0^3}{v^2}\frac{\partial^2 V}{\partial z^2} \quad (25)$$

$$\frac{\partial^2 T^*}{\partial z^{*2}} = \frac{\partial}{\partial z}\left(\frac{U_0(T_w^*-T_\infty^*)}{v}\frac{\partial \theta}{\partial z}\right)\frac{\partial z}{\partial z^*} = \frac{U_0^2(T_w^*-T_\infty^*)}{v^2}\frac{\partial^2 \theta}{\partial z^2} \quad (26)$$

Substituting equations (19), (21) and (25) into (16) yields:

$$\frac{U_0^2}{v}\frac{\partial U}{\partial z} = \frac{U_0^3}{v}\frac{\partial^2 U}{\partial z^2} - \frac{\partial \overline{uw}}{\partial z} - g\beta(T_w^* - T_\infty^*) + \frac{\sigma\mu_0^2 H_0^2(mV-U)}{1+m^2} \quad (27)$$

On rearranging equation (4.20.9) becomes:

$$\frac{\partial U}{\partial t} = \frac{\partial^2 U}{\partial z^2} - \frac{\partial \overline{uw}}{\partial z} - \frac{vg\beta(T_w^*-T_\infty^*)}{U_0^3} + \frac{\sigma\mu_0^2 H_0^2 v(mV-U)}{U_0^2(1+m^2)} \quad (28)$$

On employing non-dimensional parameters equation (28) gives:

$$\frac{\partial U}{\partial t} = \frac{\partial^2 U}{\partial z^2} - \frac{\partial \overline{uw}}{\partial z} + Gr\theta + \frac{M^2(mV-U)}{1+m^2} \quad (29)$$

where $Gr = \frac{vg\beta(T_w^*-T_\infty^*)}{U_0^3}$ and $M^2 = \frac{\sigma\mu_0^2 H_0^2 v}{U_0^2}$.

Substituting equations (20), (22) and (25) into (17) yields:

$$\frac{U_0^3}{v}\frac{\partial V}{\partial t} = -\frac{U_0^3}{v^2}\frac{\partial^2 V}{\partial z^2} - \frac{\partial \overline{uw}}{\partial z} - \frac{\sigma\mu_0^2 H_0^2 U_0(mU+V)}{1+m^2} \quad (30)$$

This on re-arranging gives:

$$\frac{\partial V}{\partial t} = \frac{1}{v}\frac{\partial^2 V}{\partial z^2} - \frac{\partial \overline{uw}}{\partial z} - \frac{\sigma\mu_0^2 H_0^2 v(mU+V)}{U_0^2(1+m^2)} \quad (31)$$

On introducing the non-dimensional parameters to equation (31) gives:

$$\frac{\partial V}{\partial t} = \frac{\partial^2 V}{\partial z^2} - \frac{\partial \overline{vw}}{\partial z} - \frac{M^2(mU+V)}{1+m^2} \quad (32)$$

where $M^2 = \frac{\sigma\mu_0^2 H_0^2 v}{U_0^2}$.

Substituting equations (23) and (26) into (3) yields:

$$(T_w^* - T_\infty^*)\frac{U_0^2}{v}\frac{\partial \theta}{\partial t} = \frac{kU_0^2}{\rho C_p}\frac{(T_w^*-T_\infty^*)}{v^2}\frac{\partial^2 \theta}{\partial z^2} - \frac{\partial \overline{wT}}{\partial z} \quad (33)$$

This on re-arranging gives:

$$\frac{\partial \theta}{\partial t} = \frac{k}{\rho C_p}\frac{1}{v}\frac{\partial^2 \theta}{\partial z^2} - \frac{\partial \overline{wT}}{\partial z} \quad (34)$$

IARJSET ISSN (O) 2393-8021, ISSN (P) 2394-1588

International Advanced Research Journal in Science, Engineering and Technology

Impact Factor 8.066 ⁜ Peer-reviewed / Refereed journal ⁜ Vol. 11, Issue 12, December 2024

DOI: 10.17148/IARJSET.2024.111201

and on introducing non-dimensional parameters equation (34) becomes:

$$Pr\frac{\partial\theta}{\partial t} = \frac{\partial^2\theta}{\partial z^2} - Pr(\frac{\partial\overline{wT}}{\partial z}) \quad (35)$$

We need to solve equations (28), (32) and (34). However, the solution of these equations is not currently possible due to the Reynolds stress terms in (28) and (32). We thus now resolve these terms first, for us to be able to work out the solution of these equations. The Reynolds stresses in (28) and (32) are respectively $\overline{(uw)}$ and $\overline{(vw)}$. We need to write this terms as functions of $x, y, U, V$, i.e we need a function $F$ such that $\overline{(uw)} = F(x, y, U, V)$ .We will adopt the Boussinessque approximation $\tau_t = -\rho\overline{uv} = A_\tau\frac{dU}{dy}$, $A_\tau$ is not a property of the fluid like $\mu$ but depends on the mean velocity $U$. We will not use the $k-\varepsilon$ model as this model assumes that a flow is isotropic hence its use is limited to such flows. We thus turn to semi empirical methods that then lead us to the study and use of the Prandtl mixing length hypothesis that for a long time has been an important tool in the analysis of turbulent boundary layers. The Reynolds shear stress $\rho\overline{uv}$ represents a flux of $x$-momentum in the $y$-direction. Prandtl assumed that this momentum was transported by eddies which moved in the$y$-direction over a distance $l$ without interaction (i.e. momentum is assumed to be conserved over distance $l$) and then mixed with existing fluid at the new location. From his experiments Prandtl deduced that:

$$\rho\overline{uv} = -\rho l^2(\frac{\partial U}{\partial y}) \quad (36)$$

At this stage further assumption is taken:
a) for $y+> 5$ we neglect the viscous term in the shear stress,
b) $l = ky$ where $k$ is the von Karman constant, sometimes referred to as the Karman constant, we thus finally have:

$$\rho\overline{uv} = -\rho k^2y^2(\frac{\partial U}{\partial y})^2 \quad (37)$$

Now (4.20.11) under (4.20.21) becomes:

$$\frac{\partial U}{\partial t} = \frac{\partial^2 U}{\partial z^2} + \frac{\partial}{\partial z}[k^2z^2(\frac{\partial U}{\partial z})^2] + Gr\theta + \frac{M^2(mU+V)}{1+m^2} \quad (38)$$

Likewise, (4.20.14) under (4.20.22) yields:

$$\frac{\partial V}{\partial t} = \frac{\partial^2 V}{\partial z^2} + \frac{\partial}{\partial z}[k^2z^2(\frac{\partial V}{\partial z})^2] - \frac{M^2(mV-U)}{1+m^2} \quad (39)$$

Equations (38), (39) and (35) in cylindrical coordinates respectively simplifies to:

$$\frac{\partial U_z}{\partial t} = V\left(\frac{\partial^2 U_z}{\partial r^2} + \frac{1}{r}\frac{\partial U_z}{\partial r}\right) - \left[\frac{1}{r}\frac{\partial\overline{U_z'U_r'}}{\partial r}\right] + Gr\theta - M^2\frac{(U_z+mU_\theta)}{(1+m^2)} \quad (40)$$

$$\frac{\partial U_\theta}{\partial t} = \left(\frac{\partial^2 U_\theta}{\partial r^2} + \frac{1}{r}\frac{\partial U_\theta}{\partial r} - \frac{U_\theta}{r^2}\right) - \left[\frac{\partial\overline{U_r'U_z'}}{\partial r} - \frac{2\overline{U_\theta'U_r'}}{r^*}\right] + M^2\frac{(mU_z-U_\theta)}{(1+m^2)} \quad (41)$$

$$\frac{\partial\theta}{\partial r} = \frac{1}{Pr}\left(\frac{\partial^2\theta}{\partial r^2} + \frac{1}{r}\frac{\partial\theta}{\partial r}\right) - \frac{\partial\overline{(U_r''\theta')}}{\partial r} \quad (42)$$

Where:

$$Gr = vg\beta\frac{T_w^* - T_\infty^*}{U_0^3}$$

$$Pr = \frac{\mu C_p}{k}$$

$$M^2 = \frac{\sigma\mu_0^2H_{0V}^2}{U_0^2}$$

IARJSET ISSN (O) 2393-8021, ISSN (P) 2394-1588

International Advanced Research Journal in Science, Engineering and Technology

Impact Factor 8.066 ⁜ Peer-reviewed / Refereed journal ⁜ Vol. 11, Issue 12, December 2024

DOI: 10.17148/IARJSET.2024.111201

With the Reynolds stresses resolved we now seek a numerical solution of equations (40), (41) and (42) subject to the boundary and initial conditions below:

**2.3 Boundary and Initial Conditions**

From equation (18) the non-dimensional form of (4) becomes:

$$t < 0 : U_z = 0, U_\theta = 0, \theta = 0 \; everywhere \tag{43}$$

$$t \geq 0: U_z = 1, U_\theta = 0, \theta = 1 \text{ at } r = \frac{1}{2} \tag{44}$$

$$U_z \to 0, U_\theta \to 0, \theta \to 0 \text{ as } r \to \infty \tag{45}$$

We need to solve equations (40), (41) and (42), subject to equations (43), (44) and (45). However, the solution of these equations is not currently possible due to the Reynolds stress terms. We thus resolve these terms first, for us to be able to work out the approximate solution of these equations by a direct numerical method. The momentum equations are resolved using Prandtl mixing length hypothesis. The Reynolds stresses in the energy conservation equation are computed in terms of Turbulent Prandtl number and Prandtl mixing length hypothesis. Thus equations (40) — (42) become:

$$\frac{\partial U_z}{\partial t} = \left(\frac{\partial^2 U_z}{\partial r^2} + \frac{1}{r}\frac{\partial U_z}{\partial r}\right) + k^2 r \left(\frac{\partial U_z}{\partial r}\right)\left(\frac{\partial U_z}{\partial r}\right) + Gr\theta - M^2 \frac{(U_z + mU_\theta)}{(1+m^2)} \tag{46}$$

$$\frac{\partial U_\theta}{\partial t} = \left(\frac{\partial^2 U_\theta}{\partial r^2} + \frac{1}{r}\frac{\partial U_\theta}{\partial r} - \frac{U_\theta}{r^2}\right) + 2k^2 r^2 \left(\frac{\partial U_\theta}{\partial r}\right)\left(\frac{\partial^2 U_\theta}{\partial r^2}\right) + M^2 \frac{(mU_z - U_\theta)}{(1+m^2)} \tag{47}$$

$$\frac{\partial \theta}{\partial t} = \frac{1}{Pr}\left(\frac{\partial^2 \theta}{\partial r^2} + \frac{1}{r}\frac{\partial \theta}{\partial r}\right) + \frac{k^2 r^2}{Pr_t}\left(\frac{\partial U_z}{\partial r}\right)\left(\frac{\partial \theta}{\partial r}\right) \tag{48}$$

$$t < 0: U_z = 0, U_\theta = 0, \theta = 0, everywhere \tag{49}$$

$$t \geq 0: U_z = 1, U_\theta = 0, \theta = 1, \text{ at } r = \frac{1}{2} \tag{50}$$

$$U_z \to 0, U_\theta \to 0, \theta \to 0, \text{ as } r \to \infty \tag{51}$$

## III. FINITE DIFFERENCE SCHEME

Considering that the systems of partial differential equations (46) — (48) are highly non-linear their solutions are approximated by finite difference method. In the following finite difference scheme the primary velocity $U_z$ is denoted by $U$ and the secondary velocity $U_\theta$ is denoted by V to reduce the subscripts as $i$ and $j$ are used as subscripts, $i$ corresponding to $r$ asj corresponds to $t$. The equivalent finite difference scheme for equations are respectively:

Where $i$ and j refer to $r$ and $t$ respectively. $r$ have been substituted with $i\Delta r$

$$U_{(i,j+1)} = U_{(i,j)} + \Delta t\left(\frac{U_{(i+1,J)} - 2U_{(i,j)} + U_{(i-1,J)}}{(\Delta r)^2} + \frac{1}{i\Delta r}\frac{U_{(i+1,J)} - U_{(i,J)}}{\Delta r}\right) + k^2 i(\Delta r)(\Delta t)\left(\frac{U_{(i+1,j)} - U_{(i,j)}}{\Delta r}\right)^2 + \Delta t\left\{Gr\theta_{(i,j)} - M^2 \frac{\left(U_{(i,j)} + mV_{(i,j)}\right)}{1+m^2}\right\} \tag{52}$$

$$V_{(i,j+1)} = V_{(i,j)} + \Delta t\left(\frac{V_{(i+1,J)} - 2V_{(i,J)} + V_{(i-1,J)}}{(\Delta r)^2} + \frac{1}{i\Delta r}\frac{V_{(i+1,J)} - V_{(i,J)}}{\Delta r} - \frac{V_{(i,J)}}{(i\Delta r)^2}\right) + 2k^2 (i\Delta r)^2 (\Delta t)\left(\frac{V_{(i+1,j)} - V_{(i,j)}}{\Delta r}\right)\left(\frac{V_{(i+1,j)} - 2V_{(i,j)} + V_{(i-1,j)}}{(\Delta r)^2}\right) + \Delta t M^2 \frac{\left(mU_{(i,j)} - V_{(i,j)}\right)}{1+m^2} \tag{53}$$

$$\theta_{(i,j+1)} = \theta_{(i,j)} + \frac{\Delta t}{Pr}\left(\frac{\theta_{(i+1,j)} - 2\theta_{(i,j)} + \theta_{(i-1,j)}}{(\Delta r)^2} + \frac{1}{i\Delta r}\frac{\theta_{(i+1,j)} - \theta_{(i,j)}}{\Delta r}\right) + \frac{k^2 (\Delta t)(i\Delta r)^2}{Pr_t}\left(\frac{U_{(i+1,j)} - U_{(i,j)}}{\Delta r}\right)\left(\frac{\theta_{(i+1,j)} - \theta_{(i,j)}}{\Delta r}\right) \tag{54}$$

IARJSET ISSN (O) 2393-8021, ISSN (P) 2394-1588

International Advanced Research Journal in Science, Engineering and Technology

Impact Factor 8.066 ⁜ Peer-reviewed / Refereed journal ⁜ Vol. 11, Issue 12, December 2024

DOI: 10.17148/IARJSET.2024.111201

The boundary and initial conditions take the form:

$$j < 0: U_{(i,j)} = 0, V_{(i,j)} = 0, \theta_{(i,j)} = 0, \text{everywhere} \quad (55)$$

$$j \geq 0: U_{(i,j)} = 1, V(i,j) = 0, \theta_{(i,j)} = 1, \text{at } i = \frac{\text{Re}}{2} \quad (56)$$

$$U_{(i,j)} \to 0, V_{(i,j)} \to 0, \theta_{(i,j)} \to 0, \text{as } i \to \infty \quad (57)$$

Using the boundary and initial conditions we determine the values for consecutive grid points for primary velocity, secondary velocities, and temperature that is $U_{(i,j+1)}, V_{(i,j+1)}$ and $\theta_{(i,j+1)}$ in component form.

The approximate solution was computed using a computer program and the results are displayed in graphs as shown in figures 4.3,4.4 4.5,4.6,4.7,4.8,4.9,4.10and 4.11

## IV. DISCUSSION OF RESULTS

The results of the simulation show the airflow velocity distribution in each airfoil that is affected by the angle of attack. With the variation of the attack angle $0^0$, $2^0$, $4^0$, $6^0$ and $8^0$, it is concluded that, the larger the angle of attack, the maximum air velocity distribution in each airfoil tends to increase

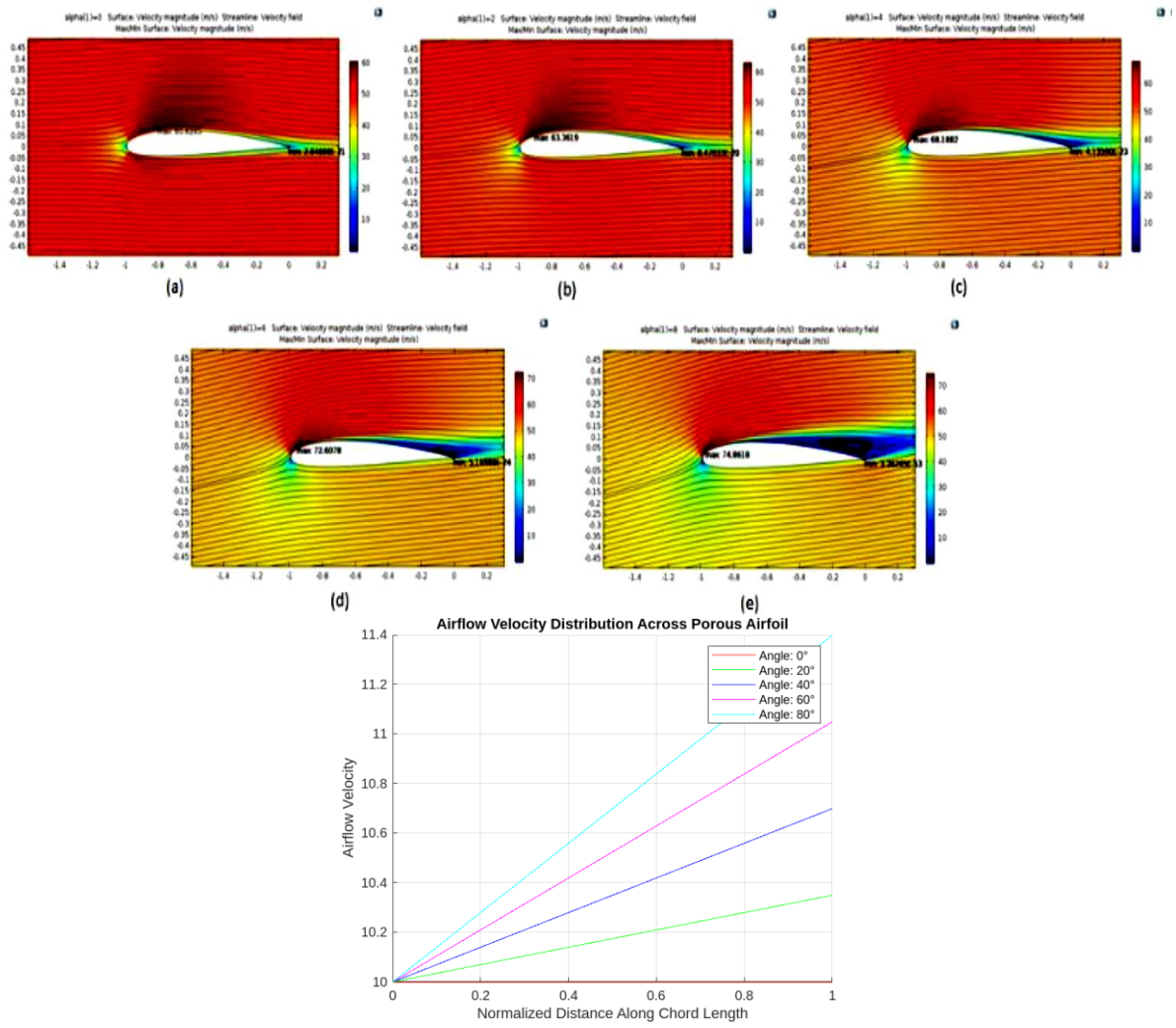


**Figure 4.3 Airflow** around the NACA Airfoil 2412 at the (a). Angle of attack 00, (b). Angle of attack 20, (c). Angle of attack 40, (d). Angle of attack 60 and (e). Angle of attack 80.

IARJSET ISSN (O) 2393-8021, ISSN (P) 2394-1588

International Advanced Research Journal in Science, Engineering and Technology

Impact Factor 8.066 ⁜ Peer-reviewed / Refereed journal ⁜ Vol. 11, Issue 12, December 2024

DOI: 10.17148/IARJSET.2024.111201

### 4.1 Primary Velocity Profiles

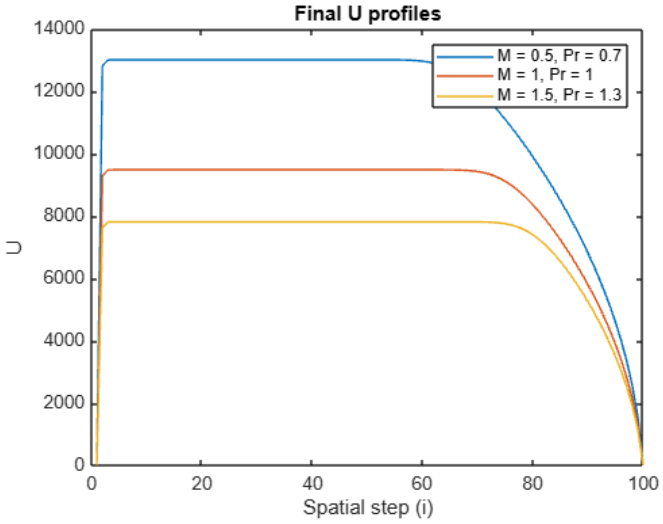


Figure 4.4 Primary velocity profiles within a moving porous aerofoil wing

From figure 4.4 it is noted that:

(i) Primary velocity is not affected by magnetic parameter and Hall parameter.
(ii) There is an increase in primary velocity profiles when Grashof number and time parameter are increased.
(iii) There is no change in primary velocity when Prandtl number is varied.

This suggests that the influence of magnetic fields on fluid dynamics in this scenario is minimal, possibly indicating that inertial forces or buoyancy effects dominate over magnetic effects. The absence of changes in primary velocity with varying Prandtl numbers suggests that the momentum diffusivity (viscosity) and thermal diffusivity (thermal conductivity) are balanced in such a way that they do not significantly affect the flow characteristics. This may imply a stable thermal regime where heat transfer does not influence momentum transfer in this particular context.

### 4.2 Secondary Velocity Profiles

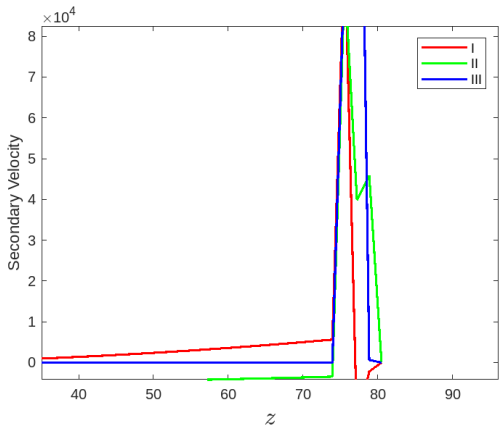


| | $M^2$ | $m$ | $Gr$ |
|---|---|---|---|
| I | 50 | 0.1 | -10 |
| II | 50 | 2 | -10 |
| III | 5 | 0.1 | -10 |
| IV | 50 | 0.1 | -1000 |

Figure4.5 Secondary velocity profiles with cooling of the wings

From figure 4.5 it is noted that:
(i) The secondary velocity profiles increase in magnitude with increase in time parameter and magnetic parameter.
(ii) Variation in Grashof number does not affect secondary velocity profiles
(iii) There is no variation in velocity profiles with variation in Prandtl.
(iv) There is decrease in the secondary velocity profiles with increase in Hall parameter.

IARJSET ISSN (O) 2393-8021, ISSN (P) 2394-1588

International Advanced Research Journal in Science, Engineering and Technology

Impact Factor 8.066 ⁜ Peer-reviewed / Refereed journal ⁜ Vol. 11, Issue 12, December 2024

DOI: 10.17148/IARJSET.2024.111201

This could indicate that the magnetic forces are enhancing the flow patterns or contributing to secondary flow structures, possibly by influencing the stability or structure of the boundary layers. Inertial or viscous forces, are more dominant in governing the secondary motion. The decrease in secondary velocity profiles with an increase in the Hall parameter suggests that the influence of the magnetic field's interaction with the charge carriers in the fluid is suppressing the secondary flow. This could be due to the Lorentz force acting in a way that dampens the secondary flow structures, indicating a complex interplay between electromagnetic forces and fluid motion.

### 4.3 Temperature Profiles

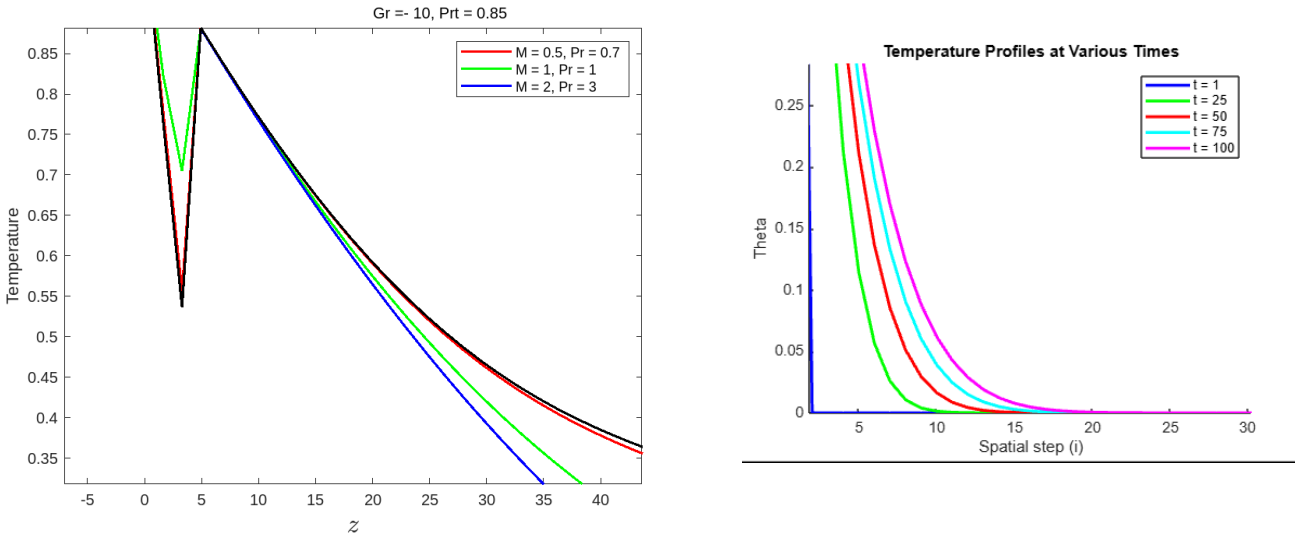


Figure 4.6 Temperature profiles

From figure 4.6 it is noted that:

(i) There is no observable variation in temperature profiles with variation in magnetic parameter and Hall parameter.
(ii) There is increase in temperature profiles with increase in time parameter.
(iii) There is decrease in temperature profiles with increase in Grashof number.
(iv) Increase in Prandtl number leads to decrease in temperature profiles.

The decrease in temperature profiles with an increase in Prandtl number indicates that as the ratio of momentum diffusivity to thermal diffusivity increases, the fluid may exhibit reduced heat transfer efficiency. This could suggest that higher viscosity relative to thermal conductivity dampens thermal fluctuations, leading to lower temperature profiles.

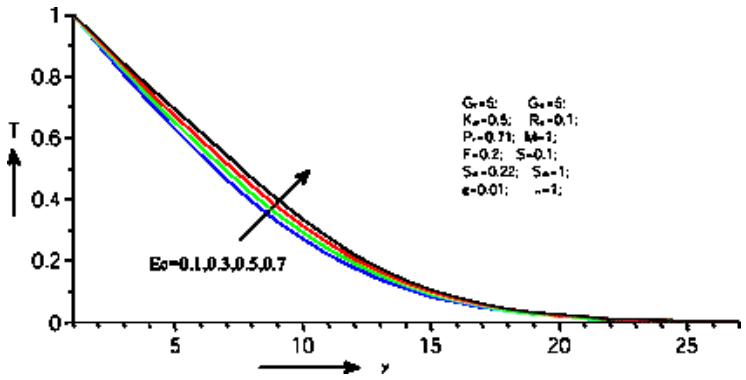


Figure 4.7 Effect of Eckert number on temperature

Velocity of the fluid reduces for increasing values of Prandtl number and magnetic parameter. Temperature of the fluid grows for rising values of Eckert number, but a reverse effect is noticed in the case of Prandtl number and radiation absorption parameter. Skin friction decreases with an increase of Eckert number and Schmidt number but a reverse effect is noticed in the case of radiation absorption parameter and magnetic parameter.

IARJSET ISSN (O) 2393-8021, ISSN (P) 2394-1588

International Advanced Research Journal in Science, Engineering and Technology

Impact Factor 8.066 ⁜ Peer-reviewed / Refereed journal ⁜ Vol. 11, Issue 12, December 2024

DOI: 10.17148/IARJSET.2024.111201

## V. CONCLUSION

The magnetohydrodynamic turbulent fluid flow over a porous aerofoil wing design within a magnetic field is numerically investigated. The effects of various flow parameters on the mean velocities and mean temperature were obtained. It is observed that increase in Grashof number led to increase in the primary velocity while there was no observable change with variation of Hall parameter.

Variation of Prandtl number significantly varied the temperature profile while it had no observable effect on the velocity profiles. Secondary velocity profiles decreased with increase in Hall parameter while there was no observable variation in temperature profiles with variation in magnetic parameter and Hall parameter.

i) It is found that the primary velocity increases with increases with increase in Grashoff number.

ii) It is found that the secondary velocity increases with decreasing magnetic parameter (M), decreases with increasing Hall parameter and the change in Grashoff number as no effect.

iii) It was also found that the temperature profile decreases with decreasing magnetic parameter (M), decreases with increasing Hall parameter and increases with decrease in Prandtl number.

## ACKNOWLEDGMENT

I gratefully acknowledge the funding received towards my MSc. from Higher Education Loans Board –(HELB), which enabled me to carry out this research.

## REFERENCES

[1]. Ahmed, T. (2013). Computational study of flow around a NACA 0012 wing flapped at different flap angles with varying Mach numbers. *Global Journals of Research in Engineering*, *13*(J4), 5-15.
[2]. Aldheeb, M. A., Asrar, W., Sulaeman, E., & Omar, A. A. (2016). A review on aerodynamics of non-flapping bird wings. *Journal of Aerospace Technology and Management*, *8*(1), 7–17.
[3]. Alsahlan, A., & Abdulkarim, T. (2017). Aerofoil design for unmanned high-altitude aft-swept flying wings. *Journal of Aerospace Technology and Management*, *9*, 335–345.
[4]. Amrit, A., Leifsson, L., & Koziel, S. (2018). Multi-fidelity aerodynamic design trade-off exploration using point-by-point Pareto set identification. *Aerospace Science and Technology*, *79*, 399–412.
[5]. Blakey-Milner, B., Gradl, P., Snedden, G., Brooks, M., Pitot, J., Lopez, E., ... & du Plessis, A. (2021). Metal additive manufacturing in aerospace: A review. *Materials & Design*, *209*, 110008.
[6]. Chebos, C., Sigey, J., Okelo, J., Okwoyo, J., & Giterere, K. (2016). Numerical investigation of unsteady MHD free convective flow past an oscillating vertical porous plate with oscillatory heat flux. *The SIJ Transactions on Computer Networks & Communication Engineering*, *04*(01), 01–09.
[7]. Chen, L., & Zonca, F. (2016). Physics of Alfvén waves and energetic particles in burning plasmas. *Reviews of Modern Physics*, *88*(1),1–12.
[8]. Cortés-Domínguez, I., & Burguete, J. (2018). Instabilities triggered in different conducting fluid geometries due to slowly time-dependent magnetic fields. *Chaos: An Interdisciplinary Journal of Nonlinear Science*, *28*(7), 075514.
[9]. Frost, W. (2013). *Heat transfer at low temperatures*. Springer Science & Business Media.
[10]. Joshi, S. N., & Gujarathi, Y. S. (2016). A review on active and passive flow control techniques. *International Journal on Recent Technologies in Mechanical and Electrical Engineering*, *3*(4), 1–6.
[11]. Keshri, O. P., Kumar, A., & Gupta, V. K. (2018). Magento-solutal convection in Newtonian fluid layer with solutal modulated boundaries. *International Journal of Non-Linear Mechanics*, *107*, 86–93.
[12]. Klose, B., Jacobs, G. B., Tank, J., & Spedding, G. (2018). Low Reynolds number airfoil aerodynamics: three different flow patterns within an angle of attack range of four degrees. In *2018 Fluid Dynamics Conference* (p. 3731).
[13]. Manda, A. Y., Chada, J. S. R., Surapaneni, S. P., & Geeri, S. (2020). Flow behaviour on aerofoils using CFD. *Journal of Mechanical Engineering, Automation and Control Systems*, *1*(1), 26–36.

IARJSET ISSN (O) 2393-8021, ISSN (P) 2394-1588

International Advanced Research Journal in Science, Engineering and Technology

Impact Factor 8.066 ⁜ Peer-reviewed / Refereed journal ⁜ Vol. 11, Issue 12, December 2024

DOI: 10.17148/IARJSET.2024.111201

## BIOGRAPHY

**GIDEON KIMUTAI KIRUI** was born in 1995 in Rift Valley Kenya. A Mathematics and Physics Teacher at Kabianga National school, Department of Mathematics and Science, he holds a First class degree in Education Science from Maasai Mara University. Being a science and engineering patron at Kabianga high school his research interests are in the areas of Differential Equations, Fluid Dynamics and Magnetohydrodynamics.

Born in 1977, Western Kenya, **Dr. Wilys Mukuna** is currently a Senior Lecturer at the Department of Mathematics, Actuarial and Physical Sciences, University of Kabianga Kenya. He holds a Doctor of Philosophy degree in Applied Mathematics from Jomo Kenyatta University of Agriculture and Technology. Engaged in teaching at both undergraduate and post graduate levels his research interests are in the areas of Computational fluid Dynamics and modelling

**Prof. Maurice Owino Oduor**, PhD, MSc, Bed Senior Lecturer is an Associate Professor of Pure Mathematics in the Department of Mathematics and Computer Science, University of Kabianga.
He is also Ag. DVC (Planning, Research and Development) of University of Kabianga
P.O.Box 2030 2030-20200 Kericho, Kenya Tel: +254721-753-991
Email: moduor@kabianga.ac.ke , moduor@kabianga.ac.ke , morricearaka@yahoo.com

  